Electronic Supplementary Material (ESI) for RSC Advances.

Electronic Supporting information (ESI)

One synthesis: two redox states.

Temperature-oriented crystallization of a charge transfer $\{Fe_2Co_2\}$ square complex in a $\{\mathbf{Fe^{II}_{LS}Co^{III}_{LS}}\}_2$ diamagnetic or $\{\mathbf{Fe^{II}_{LS}Co^{II}_{HS}}\}_2$ paramagnetic **state**.

By Siddhartha De,[a] Juan-Ramón Jiménez, ,[a] Yanling Li,[a] Lise-Marie Chamoreau,[a] Alexandrine Flambard,[a] Yves Journaux,[a] Azzedine Bousseksou,[b] and Rodrigue Lescouëzec[a]

Experimental Section and Physical Techniques

Figure S1. Perspective view of the two $\{Fe^{II}_2Co^{III}_2\}$ square units in compound **2** (top: 2a, bottom: 2b) together with atom labelling for the iron and cobalt coordination spheres

Table S1. Crystallographic parameters of compound **1** and **2**.

Table S2. Selected structural data and geometry of the square complexes in **1** and **2**.

Figure S2. Perspective view of **1** together with the intermolecular hydrogen bonding (dotted line).

Figure S3. Perspective view of the crystal packing in **2** (green crystals). The red atoms are the oxygen belonging to solvent molecules (H_2O, MeOH).

Figure S4. Solid-state UV-vis spectrum on fresh sample of **1** (red) and **2** (green) at room temperature exhibiting M-M charge transfer band.

Figure S5. (left) Temperature dependence of the absorbance at 742 nm (maximum of the Fe^{II}-Co^{III} IVCT band) ; (right) regular solution model plot based on the data obtained from temperature dependency of electron transfer equilibrium.

Figure S6. Experimental points (red points) and best-fit value (blue line) of the $\chi_M T$ *vs. T* curve of **1**.

Figure S7. Visible-near IR absorption spectra of **2** after desolvatation in the SQUID magnetometer.

Figure S8. Mössbauer spectrum at 80 K of a dried sample of **2** (desolvated at 400 K under N_2, the speed is relative to iron metal).

Figure S9. Thermo-gravimetric analysis on fresh sample of **1** (dark red) and **2** (deep green) in the 20-140 °C range at 2°C /min (under a 100ml/min nitrogen flow).

Figure S10. Plot of the $\chi_M T$ *vs. T* of **1** for a fresh sample (yellow green) and for a previously desolvated sample (red).

Figure S11. Plots of the $\chi_M T$ *vs. T* of **2** for a fresh sample (green) and for a previously desolvated sample (red).

Figure S12. $\chi_M T$ product *vs*. Irradiation time of a fresh sample of **2** at 405, 532, 808, 900 and 1313 nm at a laser power of 5, 10, 6, 7 and 7 mW/cm^2, respectively.

Figure S13. Temperature dependence of the $\chi_M T$ *product* for a fresh sample of **2** after irradiation at 808 nm (6 mW/cm^2) during 90 min.

Experimental Section and Physical Techniques

Syntheses and elemental analysis

The vbik ligand and the $PPh_4[Fe(Tp)(CN)_3]\cdot H_2O$ complex were prepared as mentioned in the literature.[S1] As vbik is light sensitive all the following reactions were performed in the dark. Elemental analysis (C, H, N) were carried out at the microanalyse service of the I.C.S.N. – C.N.R.S., Gif sur Yvette, 91198, France

$\{[Fe(Tp)(CN)_3]_2[Co(vbik)_2]\}_2(BF_4)_2\cdot 2CH_3OH$ (**1**)

A mixture of $Co(BF_4)_2\cdot 6H_2O$ (0.1 mmol) and vbik (0.2 mmol) dissolved in 10 mL methanol was added dropwise to a 10 mL methanolic solution of $PPh_4[Fe(Tp)(CN)_3]\cdot H_2O$ (0.1 mmol). The resulting deep red solution was for 30 minutes and filtered. The filtrate was poured in a crystallization dish that is covered with a parafilm with few holes and kept in a sand bath at 35 °C. Deep red prismatic crystals were obtained after 2-3 days by slow evaporation of the solution at 35 °C. Yield *ca.* 79 %.

Elemental analyses match with the fresh sample of formula: $\mathbf{1}\cdot 2CH_3OH$ calcd (%) for $C_{70}H_{68}Fe_2Co_2N_{34}O_6B_4F_8$: C 44.10, H 3.60, N 24.98; found: C 43.80, H 3.58, N 24.99.

IR (ATR): characteristic stretching vibrations were observed at 2490 (ν_{BH}), 2156, 2138 (ν_{CN}), and 1653, 1645 cm^{-1} ($\nu_{C=O}$).

$\{[Fe(Tp)(CN)_3]_2[Co(V\text{-}bik)_2]\}_2(BF_4)_2\cdot CH_3OH\cdot 10H_2O$ (**2**)

A mixture of $Co(BF_4)_2\cdot 6H_2O$ (0.1 mmol) and vbik (0.2 mmol) dissolved in 10 mL methanol was added dropwise to a 10 mL methanolic solution of $PPh_4[Fe(Tp)(CN)_3]\cdot H_2O$ (0.1 mmol). The resulting deep red solution was for 30 minutes and filtered. The filtrate was then poured in a crystallization dish covered with parafilm and kept in the fridge at 5° C. Deep green plate like crystals were obtained after one week. Yield *ca.* 70 %.

Elemental analyses match with the fresh sample of formula: $\mathbf{2}\cdot CH_3OH\cdot 10H_2O$ calcd (%) for $C_{69}H_{82}Fe_2Co_2N_{34}O_{14}B_4F_8$: C 40.34, H 4.12, N 23.18; found: C 40.70, H 4.09, N 22.05.

IR (ATR): characteristic stretching vibrations were observed at 2517, and 2502 (ν_{BH}), 2126, 2108 and 2058 (ν_{CN}), 1680 and 1672 cm^{-1} ($\nu_{C=O}$).

[S1] (a) L. Peters, M.-F. Tepedino, T. Haas, F. W. Heinemann, M. Wolf, N. Burzlaff, *Inorg. Chim. Acta,* 2011, **374**, 392 ; (b) R. Lescouëzec, J. Vaissermann, F. Lloret, M. Julve and M. Verdaguer, *Inorg*. *Chem*., 2002, **41**, 5943.

X-ray data collection and refinement

A single crystal of each compound was selected, mounted onto a cryoloop, and transferred in a cold nitrogen gas stream. Intensity data were collected with a BRUKER Kappa-APEXII diffractometer with graphite-monochromated Mo-K radiation (λ = 0.71073 Å). Data collection were performed with APEX2 suite (BRUKER). Unit-cell parameters refinement, integration and data reduction were carried out with SAINT program (BRUKER). SADABS (BRUKER) was used for scaling and multi-scan absorption corrections.

In the WinGX suite of programs[S2], the structures were solved with SIR97[S3] for **1** and SHELXT[S4] program for **2** and both were refined by full-matrix least-squares methods using SHELXL-14[S5].

All non-hydrogen atoms were refined anisotropically. Hydrogen atoms were placed at calculated positions on vbik and Tp ligands and refined with a riding model.

In **1**, H atom of the OH function of methanol molecule was located from Fourier difference map.

In **2**, the solvent region presents an important disorder. The low resolution in that region, combined with residual density prevented the location of H atoms of both MeOH and water molecules. A SQEEZE procedure was applied to this crystal structure. However, as it did not offer any significant advance in the interpretation of the crystal structure, we kept the model with disordered solvent molecules.

CCDC 1433794 - 1433795 contain the supplementary crystallographic data for this paper. These data can be obtained free of charge from The Cambridge Crystallographic Data Centre via www.ccdc.cam.ac.uk/data_request/cif.

[S2] L. J. Farrugia, *Journal of Applied Crystallogr.,* 1999, **32**, 837–838.
[S3] A. Altomare, M. C. Burla, M. Camalli, G. L. Cascarano, C. Giacovazzo, A. Guagliardi, A. G. G. Moliterni, G. Polidori and R. Spagna, *J. Appl. Crystallogr.*, 1999, **32**, 115-119.
[S4] G. M. Sheldrick, *Acta Crystallographica Section A*, 2015, **71**, 3-8.
[S5] G. M. Sheldrick, *Acta Crystallographica Section C*, 2015, **71**, 3-8.

Thermogravimetric analysis were carried out with a TGA analyzer (TAI instrument, SDT Q600) at a rate of 2 °C min^{-1} under a dinitrogen flow (100mL/min).

Solid-state UV-vis spectra were measured at room temperature on a PerkinElmer Lambda 1050 WB spectrophotometer. The measurements were performed on KBr pellets. Approximately 3 mg of fresh crystallites were mixed and grinded with *ca.* 200 mg of KBr for the measurement in the 300-1400 nm range in order to observe expected intervalence charge transfer (IVCT) transition. The pellet was then diluted (ca. 4 times) and the absorbance was measured in 300-800 nm range to obtain a better resolution on the intense absorption band observed at high energy.

FT-IR spectra were collected in the 200-4000 cm^{-1} range. Measurements were carried out on a Tensor 27 Bruker instrument working in the ATR mode (fresh samples).
The IR spectrum of the desolvated sample of **2** was recorded on KBR pellets (approximately 1 mg of desolvated sample of **2** was mixed with *ca.* 100 mg of KBr) in the 400-4000 cm^{-1} range at room temperature. The spectrum was recorded on a JASCO FTIR – 4100 spectrometer.

Variable temperature solution UV-vis spectra were recorded on a JASCO V-670 equipped with a ETC-717 Peltier module. The spectra were recorded in pure acetonitrile solutions within a temperature range of 264 K to 323 K. Samples were placed in 1 cm path length quartz cuvette and generally data were collected in the range 300-1200 nm.

Magnetic Measurments

Variable-temperature (2.0 - 400 K) magnetic measurements. Magnetic susceptibility data were collected using a Quantum Design SQUID magnetometer (MPMS5S Model) calibrated against a standard palladium sample. The magnetic susceptibility values were corrected from the diamagnetism of the molecular constituents and of the sample holder. Magnetic fields of 1 T (20-400 K) and 0.05 T (40-2 K) were used for the study. In a typical experiment, a sample is packed in a polyethylene bag which is introduced in the SQUID at 200 K under helium flow and frozen before purging under vacuum. The susceptibility measurements were carried out from 200 to 2 K, then from 2 K to 400 K, and finally from 400 to 2 K. The fresh sample were filtered from the mother solution just before the SQUID magnetometry experiment and the dehydrated samples were measured just after heating the sample in the TGA machine up to 400 K (at 2 °C/min under N_2 flow).

Photomagnetic measurements were performed on *ca*. 0.5 mg of sample. Fresh samples were introduced in the SQUID at 200 K under a helium flow and frozen before purging in order to avoid solvent loss. The irradiation was performed in the SQUID at 20 K in order to limit the effect of the heating due to the sample irradiation (H = 1 T). The relaxation of the photo-induced metastable state ($\chi_M T$ *vs* T curve) was measured at 0.5 K min.

Mössbauer spectroscopy. ^{57}Fe Mössbauer spectra of desolvated **2** were recorded using a conventional constant-acceleration-type spectrometer equipped with a 50 mCi ^{57}Co source and a flow-type, liquid-helium cryostat. The spectra were recorded at 80 K under reduced helium pressure. Least-squares fittings of the Mössbauer spectra were performed considering Lorentzian line shapes using Recoil software package.

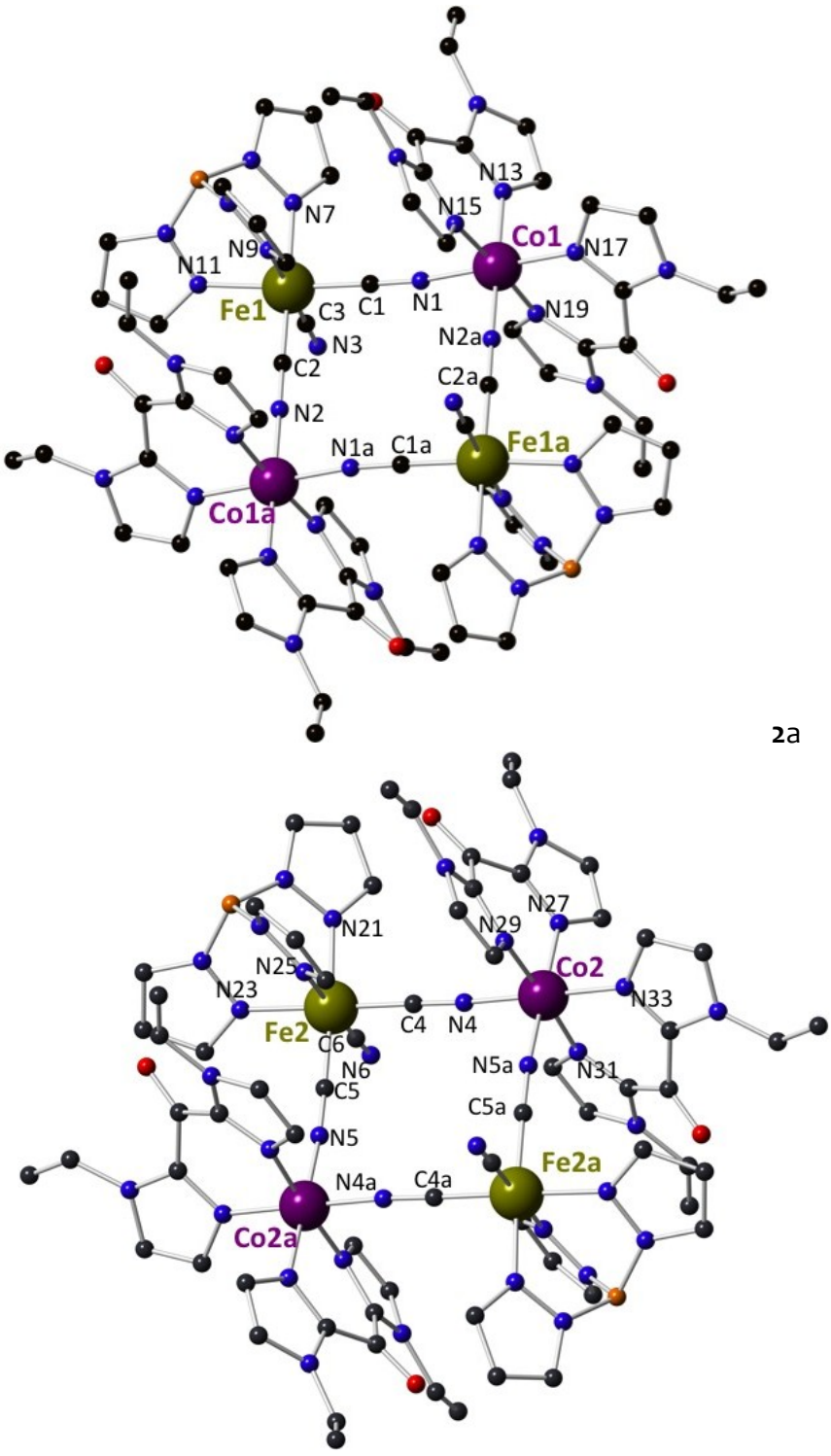

Figure S1. Perspective view of the two $\{Fe^{II}_2Co^{III}_2\}$ square units in compound **2** (top: 2a, bottom: 2b) together with atom labelling for the iron and cobalt coordination spheres (grey, blue, red, orange, yellow and purple spheres are carbon, nitrogen, oxygen, boron, iron, and cobalt atoms; hydrogen atoms are omitted for clarity). Symmetry codes: (**2**a) -x, -y, 1-z and (**2**b) 1-x, 1-y, -z.

Table S1. Crystallographic parameters of compound **1** and **2**.

	1	**2**
Formula	$C_{70}H_{68}Fe_2Co_2N_{34}O_6B_4F_8$	$C_{69}H_{82}Fe_2Co_2N_{34}O_{15}B_4F_8$
Mol Wt. [g mol-1]	1906.30	2182.98
Temperature [K]	200(2)	200(2)
space group	triclinic, P-1	triclinic, P-1
a [Å]	13.5576(4)	15.0458(3)
b [Å]	14.0743(4)	17.5052(4)
c [Å]	14.1481(4)	19.0698(5)
α[°]	115.4550(10)	85.0580(10)
β[°]	92.8150(10)	78.2870(10)
γ[°]	116.9930(10)	84.8430(10)
V [Å^3]	2069.57(11)	4886.2(2)
Z	1	2
ρ_{calcd} [gcm^{-3}]	1.530	1.366
μ[mm^{-1}]	0.829	0.710
Reflections Collected	59614	72381
Independent refrections	14369	17946
*R*1 [I≥2σ(I)]	0.0334	0.0626
*WR*2 [I≥2σ(I)]	0.0929	0.1934
GOF on F^2	1.026	1.019
CCDC	1433794	1433795

$wR2 = \{ \Sigma [w(F_o^2 - F_c^2)^2] / \Sigma [w(F_o^2)^2] \}^{1/2}$

$R1 = \Sigma \, | \, |F_o| - |F_c| \, | / \Sigma |F_o|$

Table S2. Selected structural data and geometry of the square complexes in **1** and **2**.

	1	**2**	
		Square a	**Square b**
d[Fe-$(CN)_{bridging}]_{av}$	1.915(12) Å	1.845(5) Å	1.861(5) Å
d[Fe-N(Tp)]$_{av}$	1.978(11) Å	2.000(5) Å	1.995(4) Å
d[Co-$(NC)_{bridging}]_{av}$	2.118(11) Å	1.878(5) Å	1.868(5) Å
d[Co-N(V-bik)]$_{av}$	2.123(10) Å	1.927(4) Å	1.925(4) Å
$(N\text{-}Co\text{-}N)_{av}$ bite angle	85.16 (4)°	90.05 (18)°	90.07 (18)°
$\sum_{1}^{12}\lvert 90-\alpha\rvert$ for the Fe centre	25.59 (5)°	19.98 (2)°	22.07(2)°
$\sum_{1}^{12}\lvert 90-\alpha\rvert$ for the Co centre	35.08 (4)°	16.21 (18)°	15.06 (18)°
Shape factor *S* (OC-6) for Fe centre[S2]	0.160	0.107	0.083
Shape factor *S* (OC-6) for Co centre	0.330	0.071	0.071
[Co-C-O(c=o)]$_{av}$ angle	177.05 (10)°	161.58(5)°	159.67(5)°
Interplanar dihedral angles between imidazol rings	9.71 (6) 11.08(6)	23.5(2) 23.6(2)	28.5(6) 23.7(1)
$[(NC\text{-}Fe\text{-}CN)_{bridging}]_{av}$ angle	85.65 (5)°	89.80 (2)°	89.00(2)°
$[(CN\text{-}Co\text{-}NC)_{bridging}]_{av}$ angle	92.54 (4)°	91.63 (18)°	91.79 (19)°
$[(N\text{-}C\text{-}Fe)_{bridging}]_{av}$ angle	174.53 (11)°	176.40(5)°	175.80(5)°
$[(C\text{-}N\text{-}Co)_{bridging}]_{av}$ angle	161.62 (10)°	173.65(5)°	172.96(5)°
Fe•••Co distance	5.089 Å	4.869 Å	4.867 Å

In order to better describe the geometry around Fe and Co atoms a continuous shape measures (CShM) analysis was performed.[S6] The calculated values allow to evaluate the matching between an idealized polyhedron and the actual coordination spheres. The lower the value is, the closer the actual coordination sphere to the ideal polyhedron is. CShM indicate that all the Fe and Co ions lie in slightly distorted orctahedral coordination spheres. The Shape factor (S) for the Fe centres remain low in both of the complexes, in particular for the low-spin d^6 Fe(II) ion in **2**. The measured value in **1** matches well with that observed of the PPh_4[Fe(Tp)$(CN)_3$] building block. Bigger distortions are observed in the coordination sphere of the cobalt atom in **1**, supporting the occurrence of a high-spin Co(II) ion.

[S6] a) M. Llunell, D. Casanova, J. Cirera, J. M. Bifill, P. Alemany, S. Alvarez, M. Pinsky, D. Avnir, SHAPE, v2, Barcelona, 2005; b) D. Casanova, M. Llunell, P. Alemany, S. Alvarez, *Chem. Eur. J.*, 2005, **11**, 1479.

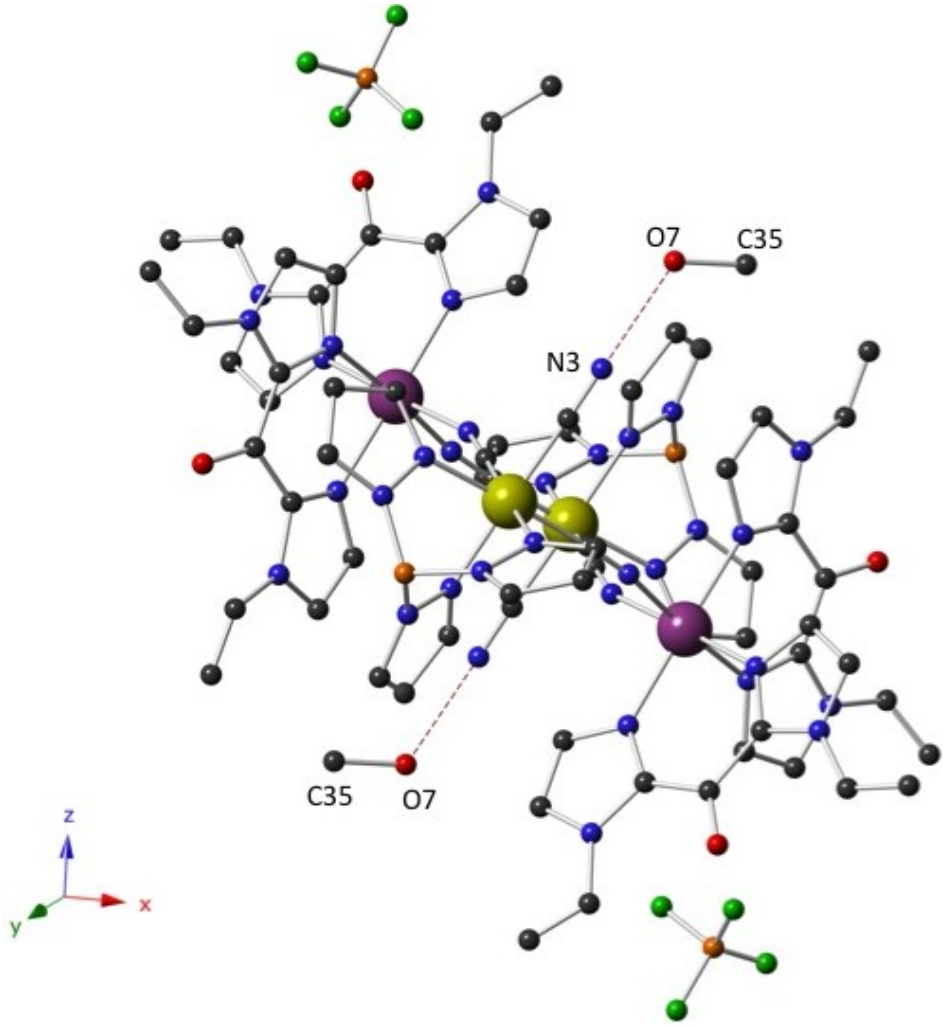

Figure S2. Perspective view of **1** together with the intermolecular hydrogen bonding (dotted line).

Atomic scheme: Fe, Yellow; Co, Violet; B, Orange; F, Green; H, Pale pink; C, Grey; N, Blue and O, Red.

$N3_{CN}$••• $O7_{MeOH}$	2.844 Å
$N3_{CN}$••• $O7_{MeOH}$ ••• $C35_{MeOH}$	105.09 °

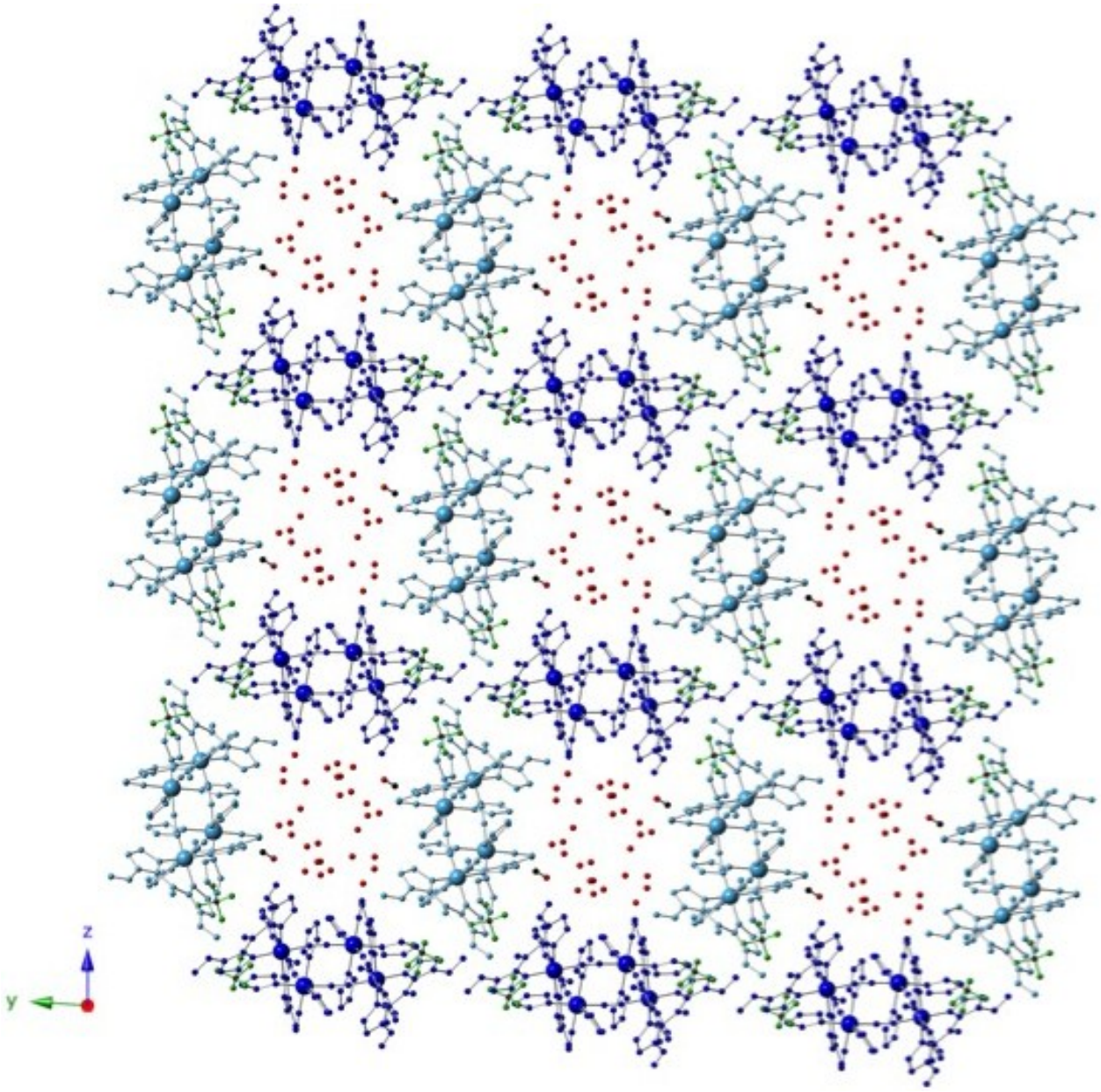

Figure S3. Perspective view of the crystal packing in **2** (green crystals). The red atoms are the oxygen belonging to solvent molecules (H_2O, MeOH). The squares **2**a and **2**b are represented in clear and deep blue, respectively and the BF_4^- anions in green. Organic ligands have been partially removed for clarity.

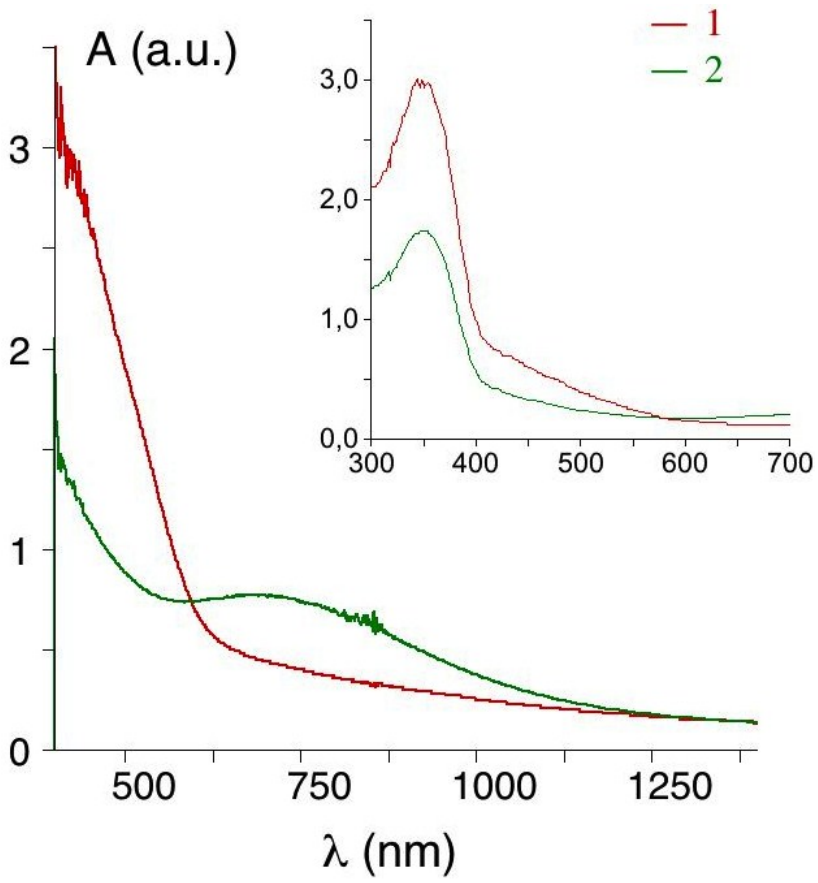

Figure S4. Solid-state UV-vis spectrum on fresh sample of **1** (red) and **2** (green) at room temperature exhibiting M-M charge transfer band.

The absorption band at 750 nm in **2** can be assigned to the Fe(II)➔Co(III) intervalence charge trasfer (IVCT) as mentioned for the previously reported dinuclear [$Fe^{II}Co^{III}$] complex and [$Fe^{II}_2Co^{III}_2$] square complexes.[S7, S8]

The absorption band in the inset for both compounds around 350 nm is most likely due to the Fe centered ligand to metal cahrge transfer(**1**) or metal to ligand charge transfer(**2**).[S8] A shoulder around 450 nm is also observed for compound **1.** According to the previously reported work this band could be assigned to the Co(II)➔Fe(III) intervalence charge transfer band. [S9]

[S7] (a) P.V. Bernhardt, F. Bozoglian, B. P. Macpherson, M. Martínez, *Coord. Chem. Rev*., 2005, 1902. (b) P.V. Bernhardt, F. Bozoglian, B. P. Macpherson, M. Martínez, *Dalton Trans*., 2004, 2582.

[S8] M. Nihei, Y. Sekine, N. Suganami, K. Nakazawa, A. Nakao, H. Nakao, Y. Murakami, H. Oshio, *J. Am. Chem. Soc.*, 2011, **133**, 3592.

[S9] D. Li, S. Parkin, G. Wang, G. T.Yee, S. M.Holmes, *Inorg. Chem.*, 2006, **45**, 1951.

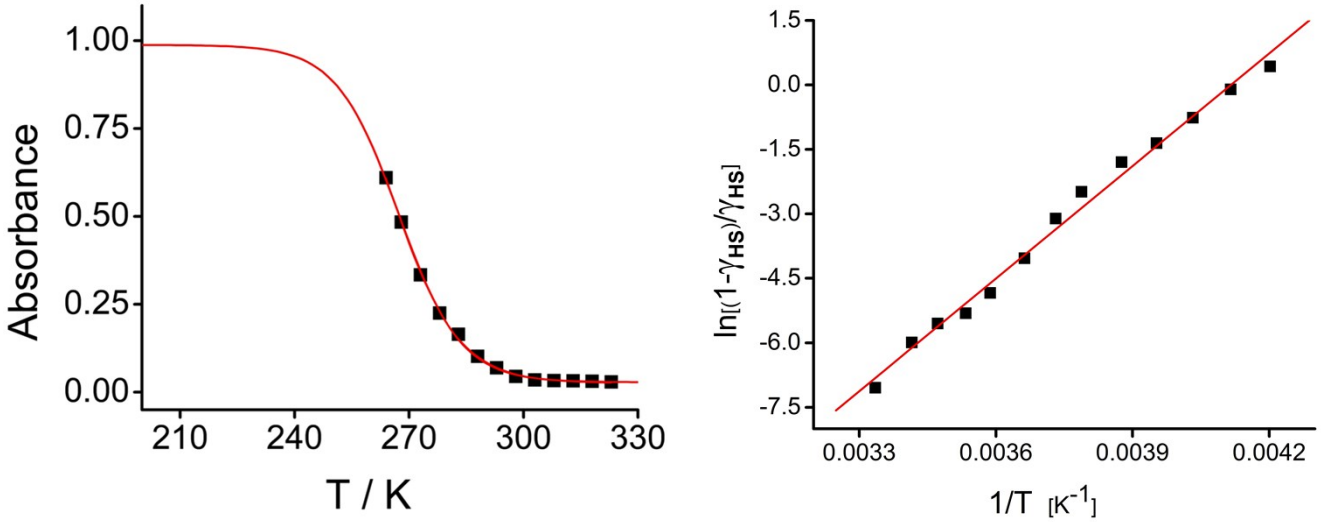

Figure S5. (Left) Temperature dependence of the absorbance at 742 nm (maximum of the Fe^{II}-Co^{III} IVCT band); (right) Linear regression based on the regular solution model applied to the UV-vis absorbance data at different temperature. The solid line (right side plot) represents the best fit.

The following equation was used in order to exctract the thermodynamic parameter associated with the electron-transfer equilibrium:[S10]

$$\ln\left[(1-\gamma_{HS})/\gamma_{HS}\right]=\left[\frac{\Delta H}{RT}-\frac{\Delta S}{R}\right]$$

ΔH, ΔS are the enthalpy, entropy variations associated with the ETCST equilibrium. R is the universal gas constant. γ_{HS} is the fraction of paramagnetic pairs (Fe^{III}-Co^{II}) and can be estimated by the relation given below:

$$\gamma_{HS}=\left[\frac{A_T-A_{LT}}{A_{HT}-A_{LT}}\right]$$

[S10] (a) C.-P. Slichter, H.-G. Drickamer, *J. Chem. Phys.*, 1972, 2142; (b) V. Niel, A.-B. Gaspar, M.-C. Muñoz, B. Abarca, R. Ballesteros, J.-A. Real, *Inorg. Chem.*, 2003, **42**, 4782; (c) B. Weber, F.-A. Walker, *Inorg. Chem.*, 2007, **46**, 6794 ; (d) P. Gütlich, A. Hauser, H. Spiering, *Angew. Chem., Int. Ed.*, 1994, **33**, 2024.

Simulation of the magnetic properties of 1 and of the desolvated phase of 2

The appropriate hamiltonian for the system is:

$H_{tot} = H_{int} + H_{so} + H_{dist} + H_{Ze}$

where the different terms have the following meaning:

$H_{int} = -J_1 (S_{Co1}.S_{Fe1} + S_{Co2}.S_{Fe2}) - J_2(S_{Co1}.S_{Fe2} + S_{Co2}.S_{Fe1})$

$$H_{so} = \sum_{i=1}^{3} -\frac{3}{2}\alpha\lambda L_{Coi}S_{Coi}$$

$$H_{dist} = \sum_{i=1}^{2} \Delta\left(L_{z\,Coi}^2 - \frac{1}{3}L_{Coi}^2\right)$$

$$H_{Ze} = \sum_{i=1}^{3}\left(-\frac{3}{2}L_{\nu\,Coi} + g_e S_{\nu\,Coi}\right)\beta.H + \sum_{i=1}^{3} + g_{eff\,Fe}(T)\beta.S_{\nu\,Fei}.H_{\nu} \quad \text{with } \nu = x,y,z$$

J_1 and J_2 are the coupling constant between the cobalt and iron ions, ⍰⍰ is the spin-orbit coupling constant of Co ions, α the orbital reduction factor and Δ the axial distortion parameter. L et S are the orbital and spin operators respectively with L = 1 and S = 3/2 in the T-P isomorphism approach.[S11] To take into account the spin-orbit coupling on the iron ions, we have introduced the spin-orbit on the iron ions using an approach close to the Lines' model with a Landé factor varying with temperature $g_{eff\,Fe}$ = F(T).[S11b]

The $g_{eff\,Fe}$(T) function has been calculated using the Curie Law for spin ½ as : $g_{eff\,Fe}^2 = \frac{4\,k\,(\chi_M.T)_{exp}}{N\beta^2}$ where $(\chi_M.T)_{exp}$ is the experimental values of Fe(TP) complex. This approach does not introduce new parameters and reduce the risk of overparametrization. The least square fit of the magnetic data for **1** gives:

J_{FeCo1} = 2.4 cm^{-1}, J_{FeCo2} = 4.7 cm^{-1}, λ_{Co} = -130 cm^{-1}, α= 0.95, Δ = -756 cm^{-1} and TIP = 114 x 10^{-6},

The agreement factor defined as $F = \frac{\sum_j \left(\chi_M.T_j^{exp} - \chi_M.T_j^{calc}\right)^2}{\sum_j \left(\chi_M.T_j^{exp}\right)^2}$ and is equal to 4 x 10^{-6}

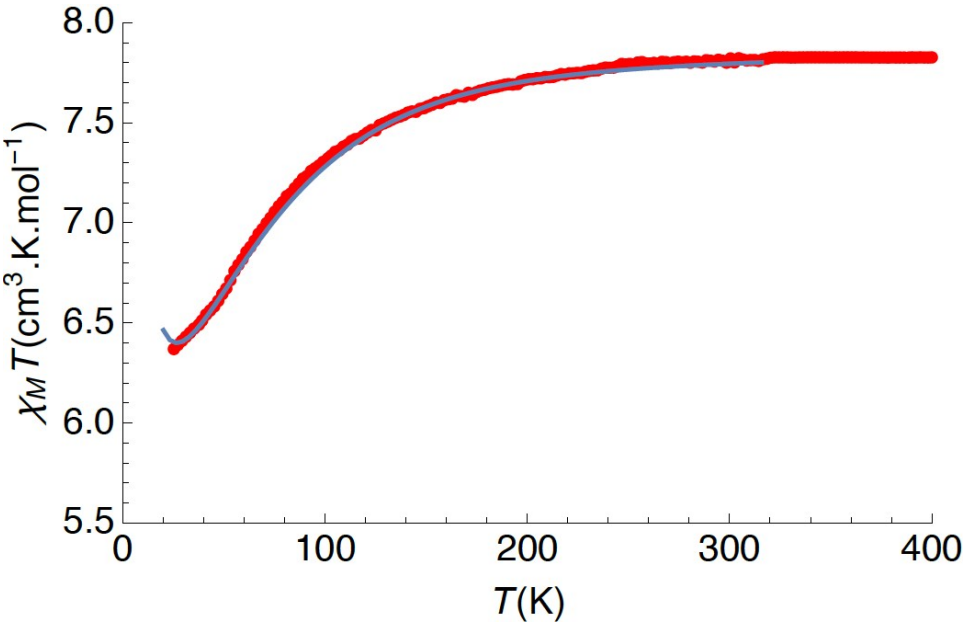

Figure S6. Experimental points (red points) and best fit values (blue line) of the $\chi_M T$ *vs. T* curve of **1**.

For **2**, as the transition is incomplete we have introduced a coefficient to take into account the low-spin diamagnetic fraction. The least square fit of the magnetic data gave J_{FeCo1} = 4.24 cm^{-1}, J_{FeCo2} = 0.06 cm^{-1}, λ_{Co} = -190 cm^{-1}, α = 0.99, Δ = -862 cm^{-1} and HS fraction = 72%. The agreement factor is equal to 2.6 x 10^{-5}.

[S11] (a) B. N. Figgis, M. Gerloch, J. Lewis, F. E. Mabbs and G. A. Webb, *J. Chem. Soc. A*, 1968, 2086-2093 ; (b) M. E. Lines, *J. Chem. Phys.*, 1971, **55**, 2977-2984 ; (c) H. Sakiyama, R. Ito, H. Kumagai, K. Inoue, M. Sakamoto, Y. Nishida and M. Yamasaki, *Eur. J. Inorg. Chem.*, 2001, 2027-2032 ; (d) F. Lloret, M. Julve, J. Cano, R. Ruiz-Garcìa and E. Pardo, *Inorg. Chim. Acta*, 2008, **361**, 3432-3445.

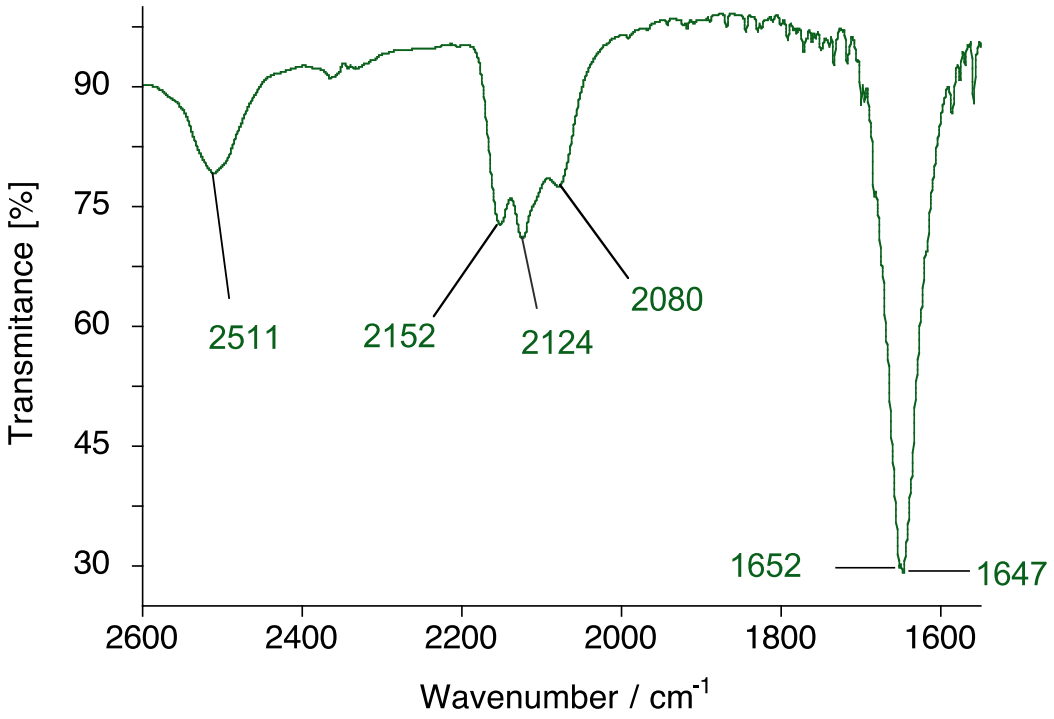

Figure S7. Visible-near IR absorption spectra of **2** after desolvatation in the SQUID magnetometer.

The number of cyanide stretching vibrations clearly increases after heating in the SQUID magnetometer (400 K under reduced helium pressure) and both peaks characteristic of Fe^{III}-CN-Co^{II}, (2154 cm^{-1}) and Fe^{II}-CN (2080 cm^{-1}) moieties are observed. The vibration located at 2124 cm^{-1} and its shoulder on the left side, are either due to Fe^{III}-CN and/or Fe^{II}-CN-Co^{III} moieties.

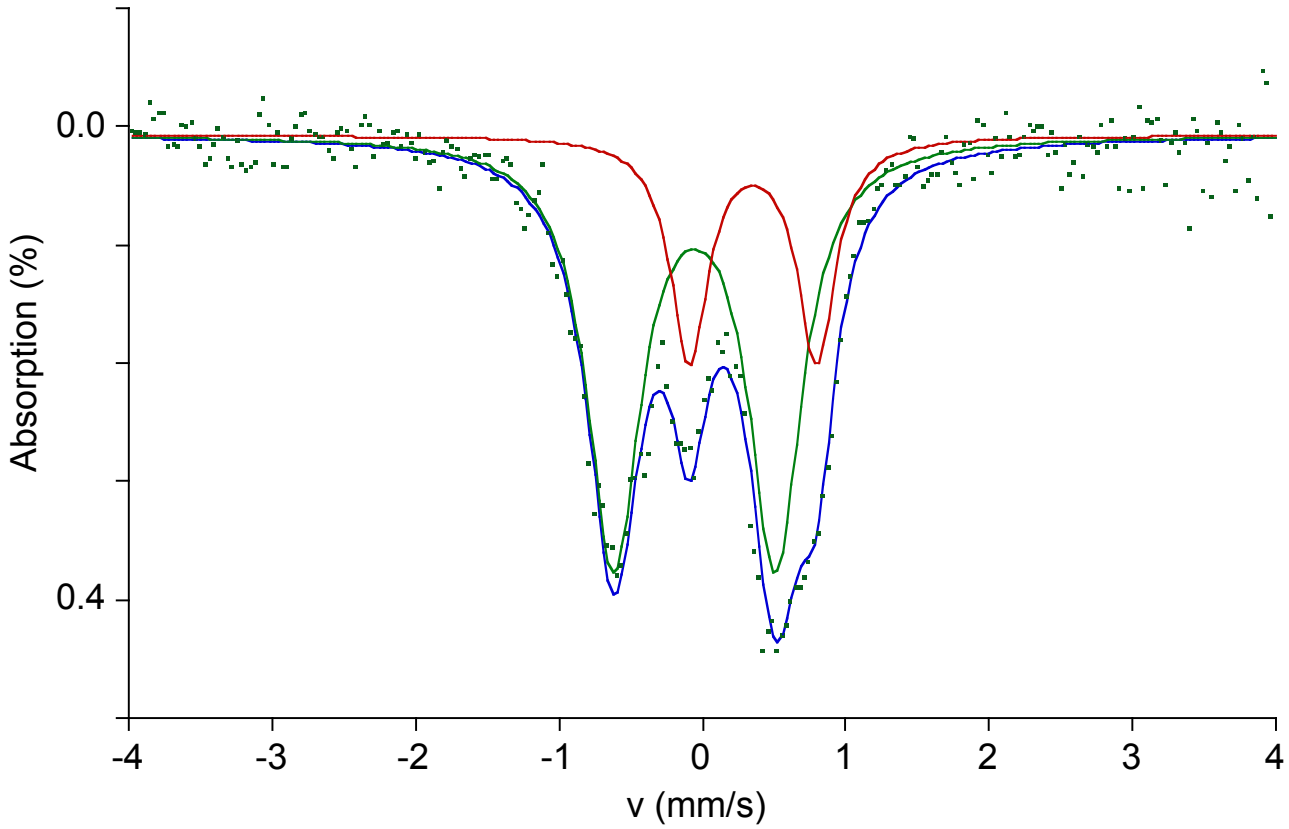

Figure S8. Mössbauer spectrum at 80 K of a dried sample of **2** (desolvated at 400 K under N_2, the speed is relative to iron metal).

Site Parameters

	IS (mm/s)	**QC (mm/s)**	**A (counts·mm/s)**	**w+ (mm/s)**
Fe^{II}_{LS} (red)	-0.054(11)	1.128(17)	100400(8200)	0.223(18)
Fe^{III}_{LS} (green)	0.354(16)	0.887(27)	37800(6600)	0.159(26)

Compiled Site Populations (%)

Fe^{II}_{LS} (red)	72.6(59)
Fe^{III}_{LS} (green)	27.4(48)

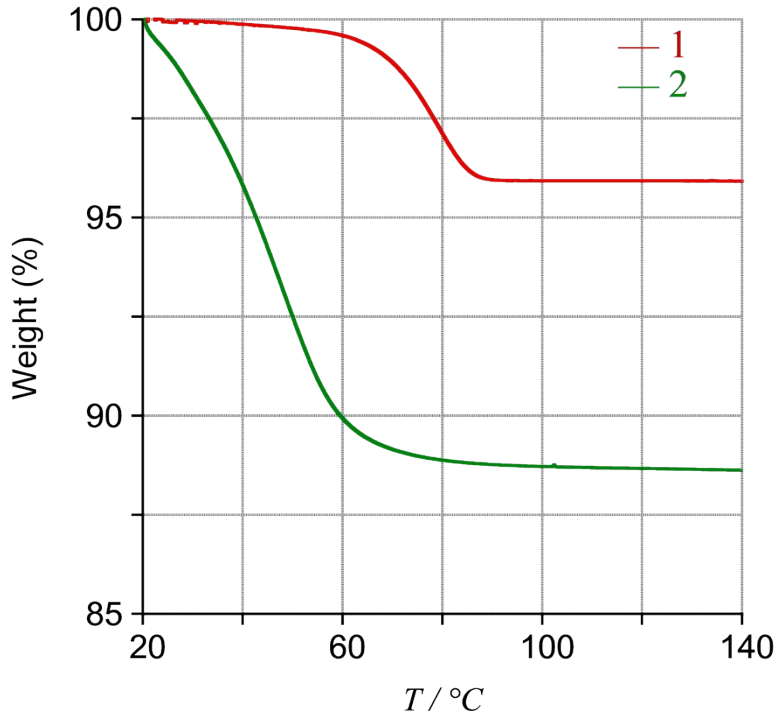

Figure S9. Thermo-gravimetric analysis on fresh sample of **1** (dark red) and **2** (deep green) in the 20-140 °C range at 2°C /min (under a 100ml/min nitrogen flow).

Compound **1** exhibits a slight weight loss of 0.50 % from room temperature to 55 °C, which is most probably due to the loss of adsorbed solvent molecule from surface of the crystals or in other words solid wetting. More interestingly, a significant weight loss (about 3.5 %) is observed from 55 °C to 95 °C. It is ascribed to the loss of the two methanol molecules (theoretically 3.35 % of sample weight), which are hydrogen bonded with the square compound. At higher temperatures (> 100°C), the compound is stable under nitrogen atmosphere up to at least 140 °C.

Compound **2** exhibits a significant weight loss from room temperature up to 85 °C, which corresponds to about 10.4 % of the initial sample mass. This weight loss matches well with the removal of the solvent molecules (ten water and one methanol molecules would correspond to a 10.3 % of the sample weight). At higher temperatures, the compound is stable under nitrogen atmosphere at least up to 140 °C.

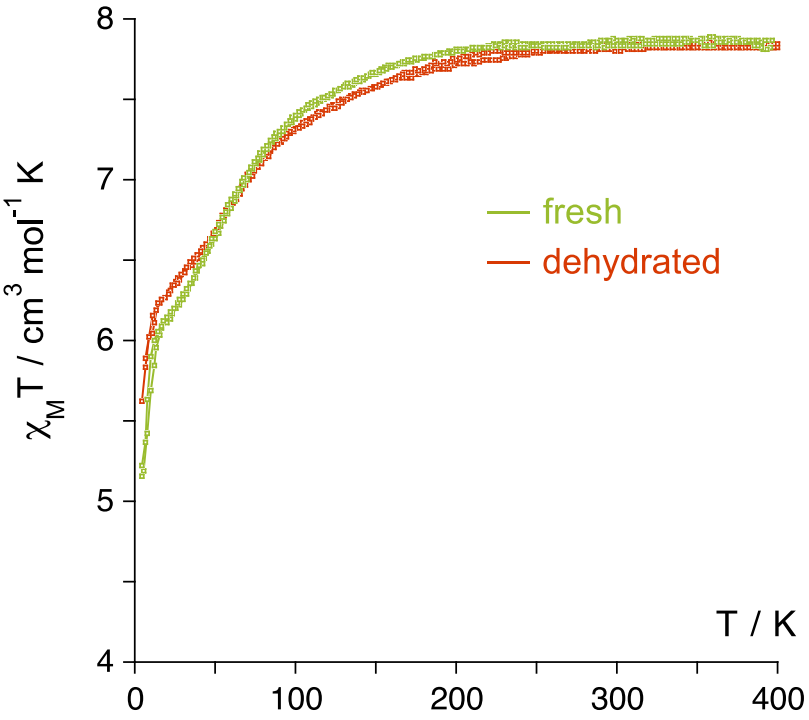

Figure S10. Plot of the $\chi_M T$ *vs. T* of **1** for a fresh sample (yellow green) and for a previously desolvated sample (red).

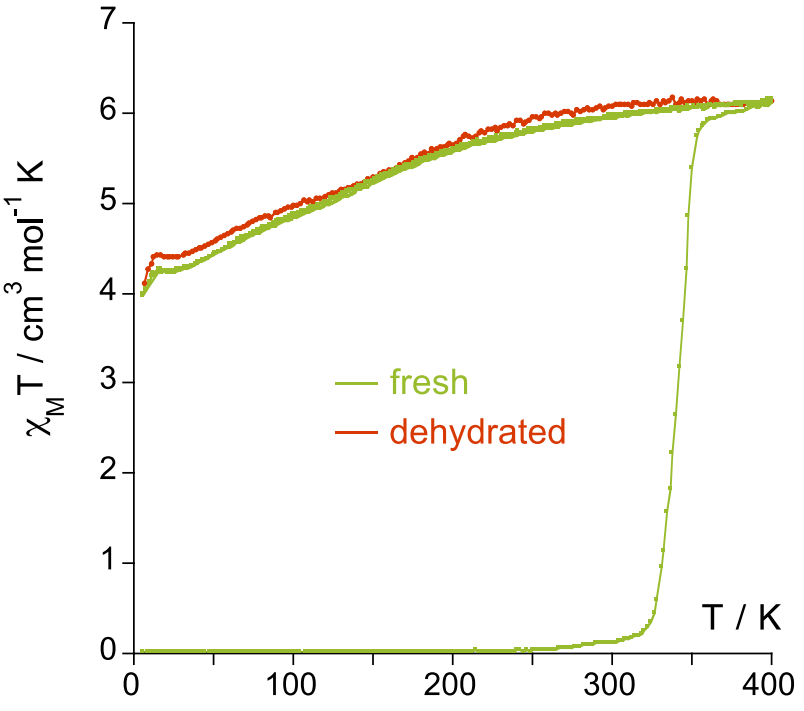

Figure S11. Plots of the $\chi_M T$ *vs. T* of **2** for a fresh sample (green) and for a previously desolvated sample (red).

Both compounds were desolvated in the TGA machine under a N_2 flow.

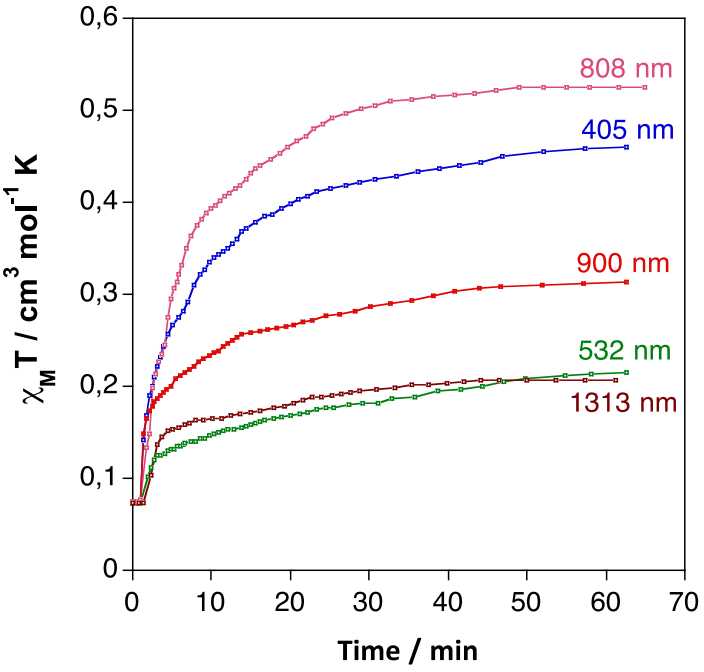

Figure S12. $\chi_M T$ product vs. Irradiation time of a fresh sample of **2** at 405, 532, 808, 900 and 1313 nm at a laser power of 5, 10, 6, 7 and 7 mW/cm^2, respectively.

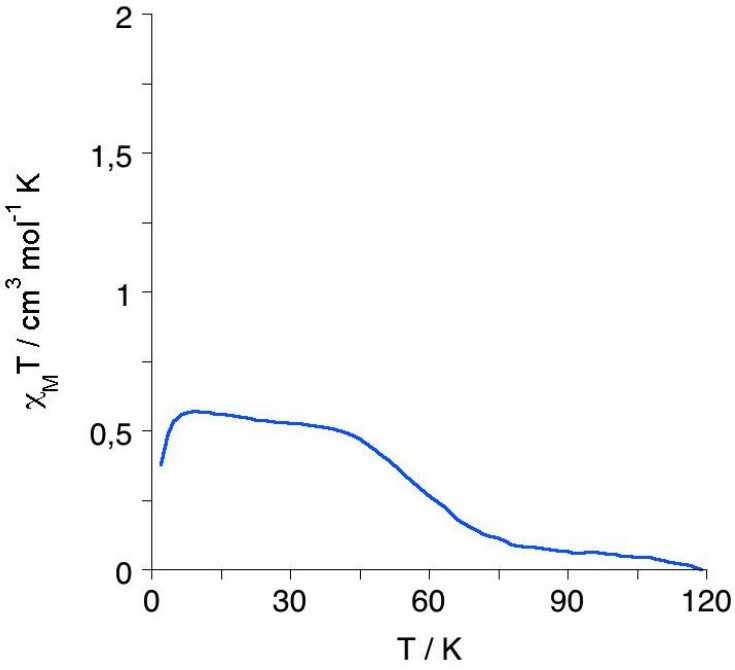

Figure S13. Temperature dependence of the $\chi_M T$ *product* for a fresh sample of **2** after irradiation at 808 nm (6 mW/cm^2) during 90 min.

Note: The photo-induced paramagnetic state was obtained by irradiating the sample at 20 K during 90 minutes. Then the laser light was switched off and the $\chi_M T$ product was measured from 2 K to 120 K at 0.3 K /min. The thermal relaxation of the photo-induced metastable state occurs near T_{LIESST} = 60 K in the present experimental conditions.